REGIONAL WORKSHOP
TRANSPORT RESEARCH AND BUSINESS COOPERATION IN SEE
6 - 7 December 2010, Sofia

TRAM VEHICLE MOVEMENT SAFETY

Dobrinka Atmadzhova **Emil Mihaylov**
atmadzhova@abv.bg emm_1968@abv.bg

University of Transport (VTU Todor Kableshkov),
Department of Transport Equipment
158 Geo Milev Street, Sofia 1574, Bulgaria

Abstract

Urban rail vehicles can present peculiar problems that require specific analysis of both vehicle dynamics and wheel–rail contact phenomena. It is necessary to study the effect of track geometrical defects on running safety of tramcar vehicles. This article deals with the numerical experimental investigations that were performed to evaluate derailment risk, showing the mechanism of flange climb and the conditions that can mainly influence derailment occurrence. In particular, the influence of the dynamic effects related to the vehicle response to track irregularities is investigated, showing that the track geometrical defects play a key role with respect to derailment risk. The main object of study is trams used to service tthe urban transport system in Sofia. In order to avoid the beginning and/or the growth of the dangerous vehicle–track dynamic interaction phenomena, the operator and the vehicle manufacturer should cooperate: the operator can make a survey on the track maintenance conditions to check the presence of critical perturbations with respect to the vehicle fleet characteristics, the vehicle manufacturer can verify at design stage if the tramcar suspension should be optimized to reduce sensitiveness to specific track features.

Keywords: *Tram vehicle, Wheel–rail contact, Track irregularity, Flange climb derailment*

1. INTRODUCTION

This article deals with vehicle safety towards flange climb derailment, focusing on the influence of the dynamic effects related to the response to the track irregularities.

During the last two years, University of transport and Metropolitan Electrical Transport - Sofia have been extensively involved in the numerical and experimental analysis of the dynamic behavior of urban rail vehicles.

Flange climb derailment risk is usually assessed through Nadal's criterion [3, 6], which is based on a single wheel lateral to vertical force ratio (**L/V**) and allows us to identify the limit value for the same ratio. Other flange climb derailment criteria have been proposed recently [4], which include an **L/V** distance limit and consider the effect of the wheelset angle of attack. The contribution of this article is to point out that, for proper analysis of the derailment phenomenon, it is not sufficient to define the **L/V** limit, which corresponds to a specific geometry of the wheel–rail coupled profiles and to a given friction coefficient. When dealing with the real situation of a tramcar running on an irregular track, the dynamic effects related to the vehicle response to track perturbations must also be carefully taken into account.

In order to investigate this topic, after showing the characteristics and capabilities of the developed urban vehicle numerical simulator, the results of a parametric analysis on the influence of track geometrical defects on flange climb derailment are presented. Reference is made to a vehicle operated in the BG, which has been both extensively tested and numerically simulated.

2. Vehicle model

All the analyses presented in this article are performed by means of a non-linear mathematical model that includes a full schematization of the vehicle and an accurate description of the contact forces [1].

The mathematical model of the vehicle is based on a multi-body, large-displacement schematization, where kinematic non-linearities are fully accounted for. It allows us to analyse the non-stationary behavior of a tramcar, running in a tangent and curved track, with a variable speed. Combined longitudinal, lateral, and vertical vehicle motion is considered.

With the aim of reproducing the most common configurations of modern vehicles, the numerical model has been designed to allow various combinations of basic modules. The different modules can be linked, one to the other, by means of kinematic constraints and/or elastic elements, reproducing the actual connections between carbodies.

In order to fit the different structural arrangements adopted for bogies (especially articulated bogie frames) and wheelsets (e.g. elastic wheels), a model superposition approach is adopted: the equations of motion are written in terms of the generalized coordinates, corresponding to the rigid and flexible natural modes of each module component (carbody, bogie, and wheelset), considered free from any mutual/global constraint. The single components are then coupled by means of elastic and damping elements, reproducing the primary and secondary suspensions.

The equations of motion of the complete vehicle [1] are obtained applying Lagrange's equations. The final expression of these equations can be written in the following matrix form:

$$\begin{aligned} &\mathbf{M}(\mathbf{x})\ddot{\mathbf{x}} + \mathbf{C}\dot{\mathbf{x}} + \mathbf{K}\mathbf{x} = \mathbf{Q}(\mathbf{x}, \dot{\mathbf{x}}, t) \\ &\mathbf{Q} = \mathbf{Q}_m + \mathbf{Q}_c + \mathbf{Q}_{nl} + \mathbf{Q}_{cf} \end{aligned} \tag{1}$$

where $\mathbf{x}$ is the vector containing the whole model independent variables; $\mathbf{M}$, $\mathbf{C}$, and $\mathbf{K}$ are the mass, damping, and stiffness matrices of the whole tramcar model; vector $\mathbf{Q}$ contains the generalized forces associated with the non-linear terms related to the vehicle's inertia $\mathbf{Q}_m$, the connections between carbodies $\mathbf{Q}_c$, the effects of non-linear elastic elements (e.g. bumpstops) $\mathbf{Q}_{nl}$, and the non-linear wheel–rail contact forces $\mathbf{Q}_{cf}$, which also account for track irregularity excitation.

In this article, reference is made to a particular urban rail vehicle – tramcar **type** T8M 700 IT (figure 1) which is composed of three carbodies and four bogies. The two bogies (figure 2) at the extremities are traditional ones, with motorized solid axles, and two bogies (figure 3) at the extremities in body "C" are traditional ones, solid axles.

With this design choice, the vehicle becomes partially low-floor.

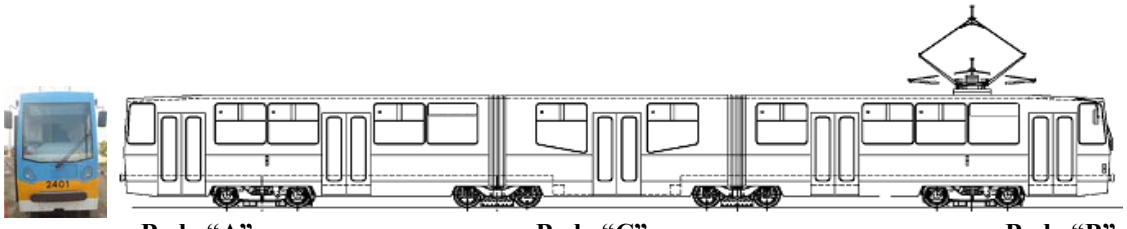

Figure 1. The urban rail vehicle.

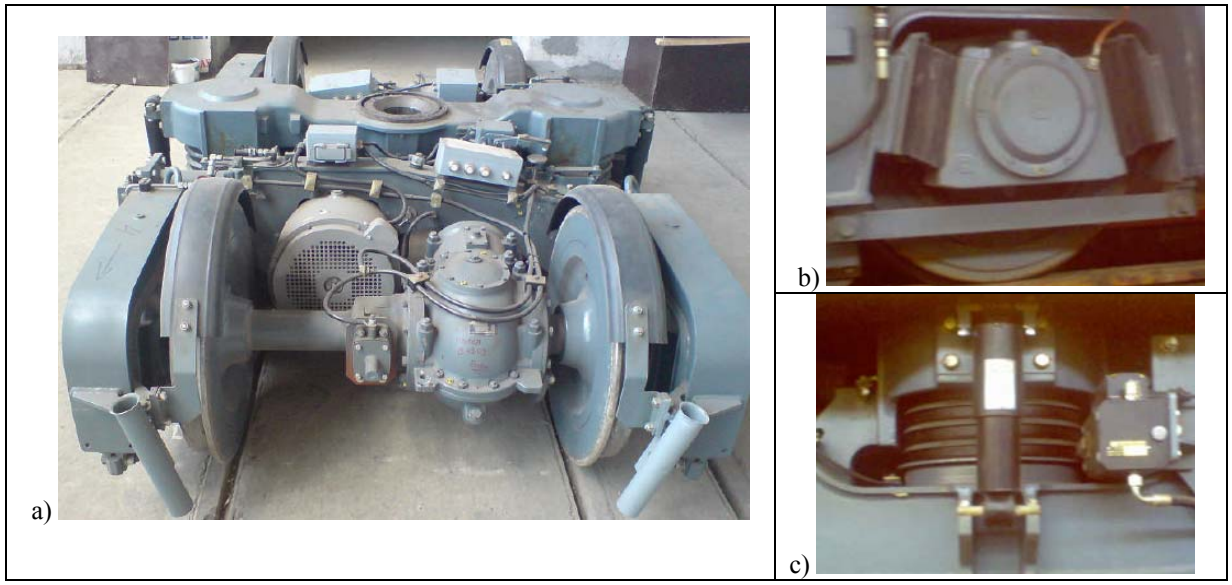

Figure 2. The bogie with motorized solid axles in urban rail vehicle.
(a – the bogie; b - the firstly suspension; c - the secondary suspension)

Figure 3. The bogie at the extremities in body "C" urban rail vehicle.

3. WHEEL–RAIL CONTACT MODEL

The contact model adopted for the calculation of the forces acting at the wheel–rail interface is suitable for reproducing the contact phenomena, which are typical of tramcar operation. In particular, it is designed to account for the out-of-plane contacts, which occur as a consequence of the not negligible angles of attack in lowradius curves; as well as for the presence of multiple contact patches on the tread and the flange [2, 5, 9].

The normal forces are evaluated through a multi-Hertzian model [7], whereas Shen-Edrick- Elkins formulation [8] is used to calculate the forces acting in the tangential plane.

When dealing with sharp curves, the longitudinal position of the flange contact point on the guiding wheel can move forward or backward, with respect to the wheel's centre, depending on the wheel–rail angle of attack (figure 4). If a forward shift occurs, as a consequence of the resulting downward speed component, an uplift creep force arises. This force may be responsible for flange climb, especially if combined with severe track irregularity conditions.

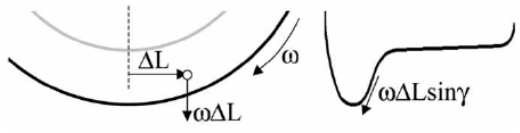

Figure 4. Effect of the longitudinal position of the flange contact point.

4. EXPERIMENTAL VALIDATION

For the considered vehicle, several experimental data were collected during measurements carried out in both real operation and particularly severe conditions, on a test track. The test track consists of a railway test section **~ 400 m** long, which includes the central portion, a right curve (**800 m** radius). At the curve's mid-length, the track presents an artificial defect, which consists of a local in-phase alignment and a cross-level perturbation, **10 m** long, with maximum amplitude of **45 mm** and **25 mrad**, respectively (figure 5).

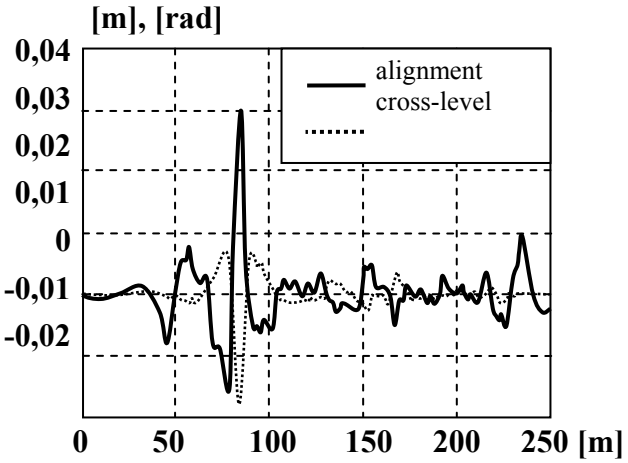

Figure 5. Test-track artificial defect. Measured track geometry: alignment and cross-level.

The test runs were also simulated through the numerical model presented in sections 2 and 3: measured data were considered for test-track geometry, wheel and rail profiles (maximum flange contact angle γ_{max} = **73°**) and friction coefficient (**μ = 0,5**).

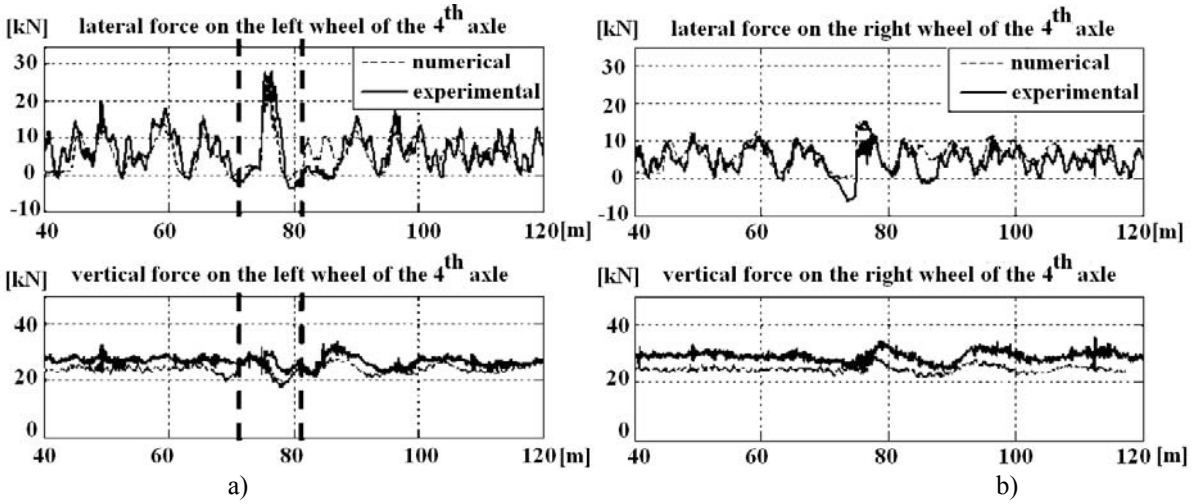

Figure 6. Numerical–experimental comparison: contact forces on the two wheels of the fourth axle.

Figures 6 and 7 show an example of numerical–experimental comparison: they refer to the lateral and vertical forces acting on the two wheels of the fourth axle and to the carbody-bogie relative motion, when the vehicle crosses the track perturbation at **35 km/h** (figure 7(a)). The position of the perturbation is indicated in figure 6(a) by the band between the two vertical dashed lines. As it can be observed, the numerical simulation is in very good agreement with the experimental data. In particular, the numerical model accurately reproduces the peak in the left wheel lateral contact force (figure 6(a)).

Flange climb derailment risk is usually assessed through Nadal's criterion, which allows us to identify the limit value of the lateral to vertical force ratio **L/V**, as a function of the friction coefficient μ at the wheel–rail interface and of the flange maximum contact angle γ_{max}:

$$\left(\frac{L}{V}\right)_{lim} = \frac{\tan\gamma_{max} - \mu}{1 + \mu\tan\gamma_{max}} \qquad (2)$$

The formula above is based on the following hypotheses:

- presence of a single-contact point on the flange;
- longitudinal creep force negligible (rigorous for independently rotating wheels with no driving/braking torque applied);
- transversal creep force in saturation.

Given the importance of Nadal's criterion in derailment analysis, the capability of the numerical model to correctly reproduce the measured **L/V** ratio is essential. Figure 7(b) shows the comparison between the numerical and experimental time histories of the **L/V** ratio. In this case, a very good agreement between numerical results and experimental data can also be observed.

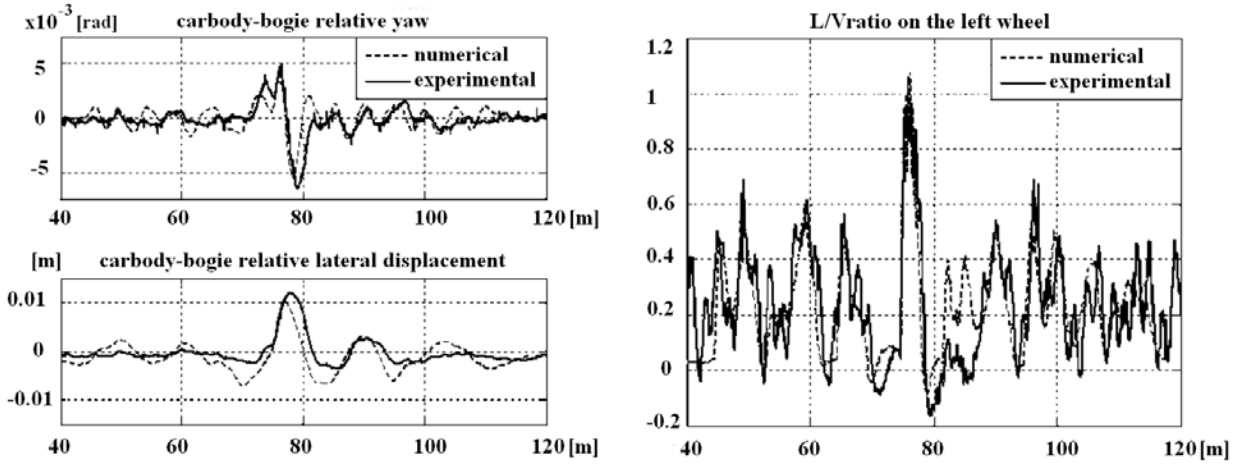

a) b)

Figure 7. Numerical–experimental comparison:
(a) carbody–bogie relative motion; (b) **L/V** ratio on the left (outer) wheel of the fourth axle.

5. DERAILMENT SIMULATION

The derailment was not reached during test-track experimental runs for evident safety reasons.

Nevertheless, once validated, the numerical model can be valuably adopted for virtual simulation of the derailment event. To this end, numerical simulations were performed in different operating conditions, considering the real track irregularity.

As an example, the numerical results relevant to a **350 m**-radius left curve, with **0,15m** superelevation, negotiated at **74 km/h**: these results refer to the central bogies. Measured irregularity data were given as input to the simulations.

Making a zoom on the last second of simulation (figure 8), it can be noticed that contact on the tread is lost for the first time around **6,4 s**, but then the wheel falls again on the rail. On the contrary, the second loss of contact on the tread, at **7 s**, leads to the derailment.

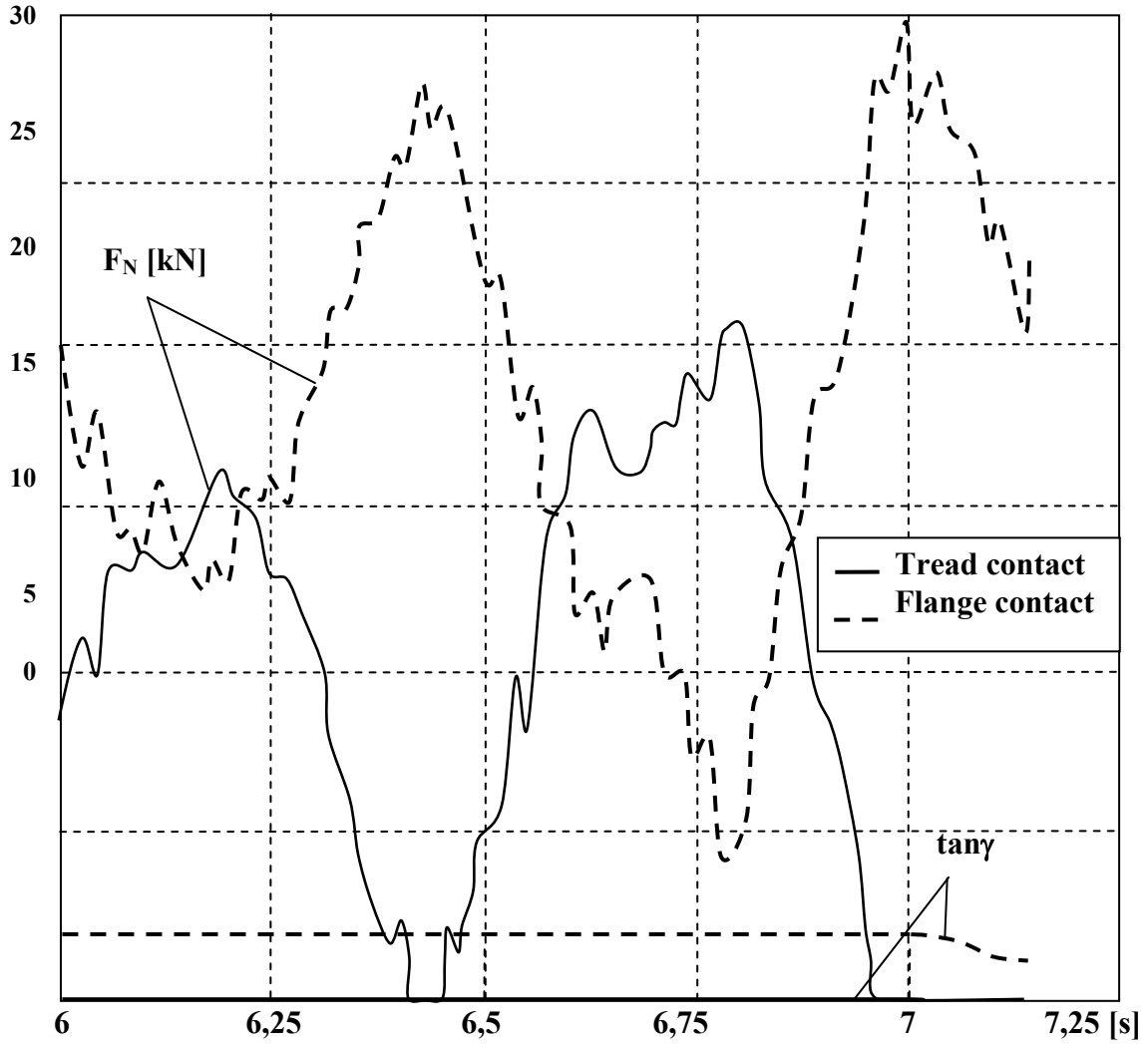

Figure 8. Derailment simulation, **V = 74 km/h**, **R = 350 m**, and super-elevation **h = 0.15 m**: zoom of the normal contact forces – $\mathbf{F_N}$, and contact angle on the front outer wheel - **tanγ**.

It is interesting to look at figure 8 together with the time history of the contact angle. Owing to the specific geometrical characteristics of the coupled profiles, as soon as the flange contact appears (**1.5 s**), the maximum contact angle (γ_{max} **= 63°**) is reached and remains constant during all the curve, until the derailment occurs (**7 s**). At this time, the contact angle suddenly decreases, as the wheel is climbing on the rail.

Considering the time history of the **L/V** ratio on the outer wheel (figure 9), whenever the tread contact is lost (**6.4** and **7 s**), Nadal's limit is reached, showing that, as expected, this criterion is definitely appropriate for detection of danger. Whether this danger corresponds or not to the actual flange climb (depending on the vehicle dynamic response to track excitation), it is not that important, as safe operation requires proper margin on the **L/V** ratio. In conclusion, Nadal's criterion can be considered as an efficient practical tool to assess the derailment risk in case of independently rotating wheels.

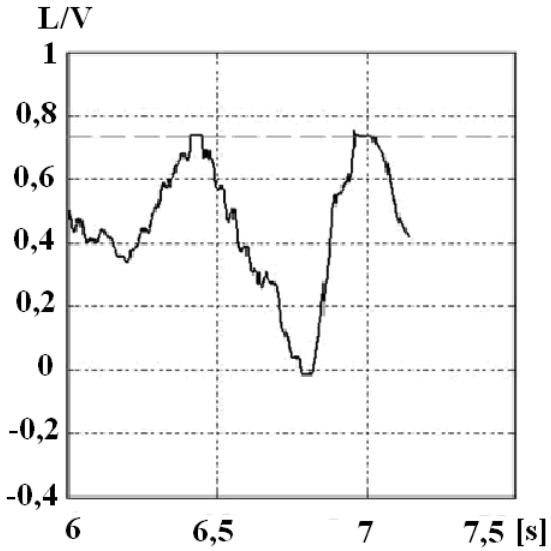

Figure 9. Derailment simulation, **V = 74 km/h**, **R = 350 m**, and super-elevation **h = 0.15 m**: **L/V** ratio on the front outer wheel.

6. INFLUENCE OF TRACK IRREGULARITY ON DERAILMENT RISK

The example of derailment simulation shownin section 6 clearly shows that the dynamic effects related to track irregularities excitation are of fundamental importance for the derailment phenomenon. This is the reason it has been decided to perform a parametric analysis on the influence of track geometrical defects. Considering the vehicle under study, various simulations were performed, assuming different track irregularity input and vehicle speeds. A number of sample track perturbations were generated, by varying the following parameters: cyclic or local defects, various amplitudes, and various wavelengths.

The simulations were performed both in curve (the reference curve has **300 m** radius and **50 mm** superelevation) and tangent track: in the first case, the highest speed considered was **55 km/h** (which is the maximum allowable speed for the considered curve), while in the second case, the speed was varied in the range of **40–90 km/h**. In all the simulations, fixed friction coefficient (**μ = 0.5**) and wheel–rail profiles (maximum flange contact angle **γ = 73°**) were assumed.

First of all, a local alignment perturbation with fixed length (**10 m**) and variable amplitude (Table 1) was considered. Figure 10 summarizes the results of the performed simulations in curve: it represents the vehicle response, in terms of the maximum **L/V** ratio calculated on the fourth axle, as a function of speed. As it can be observed, the maximum **L/V** ratio increases with the increasing speeds. For the bigger amplitude (level three) and the highest speed (**55 km/h**), the maximum **L/V** reaches Nadal's limit, for the considered wheel profile and friction coefficient, and derailment is achieved in the corresponding simulation.

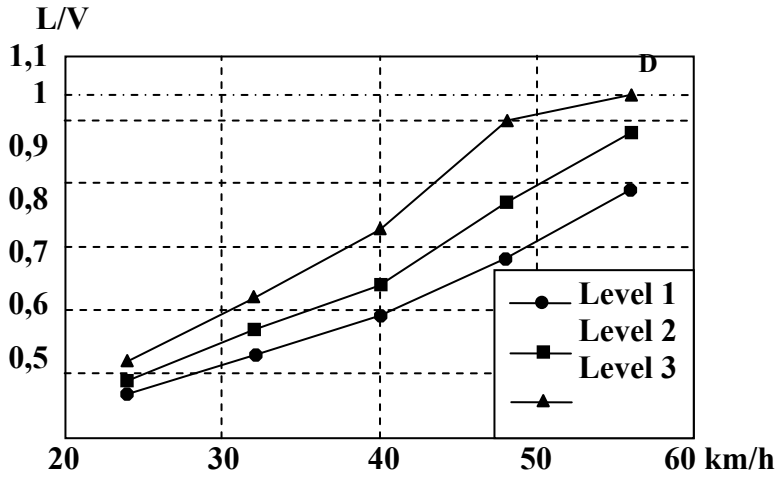

Figure 10. Vehicle response to local alignment perturbation in curve: maximum **L/V** ratio on the fourth axle as a function of speed (defect amplitudes according to table 1).

Table 1. Considered defect amplitudes for both local and cyclic alignment perturbations.

Levels	Alignment defect amplitude
Level 1	**16 mm**
Level 2	**22 mm**
Level 3	**32 mm**

The situation of a single local perturbation is not always the most realistic one. In fact, high geometrical defects with almost-cyclic pattern can often be observed on urban tracks. Typically, cyclic irregularities may arise because of some particular evolution of the track geometry, especially as a consequence of vehicle-infrastructure dynamic interaction.

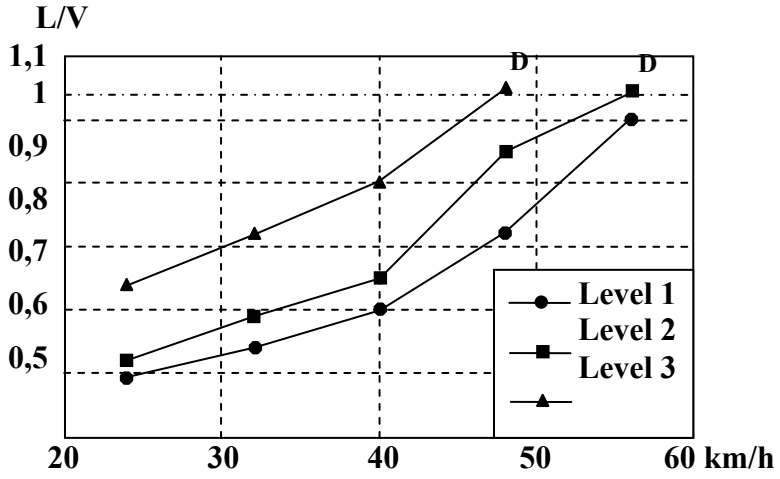

Fig. 11. Vehicle response to cyclic alignment perturbation in curve: maximum **L/V** ratio on the fourth axle as a function of speed (defect amplitudes according to table 1).

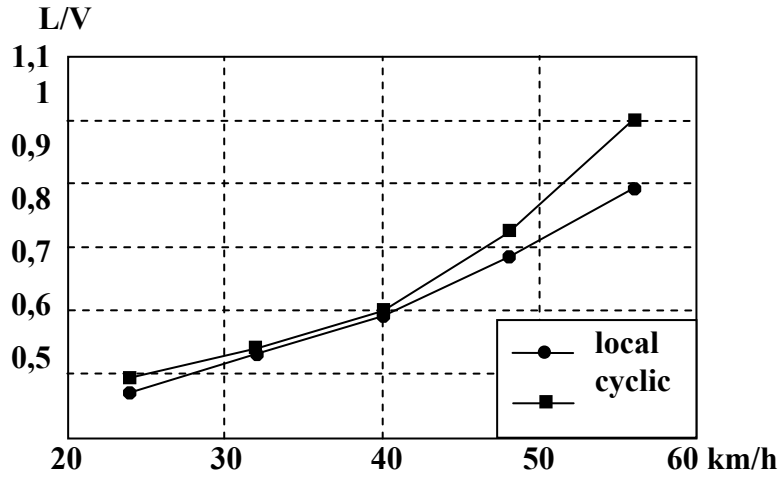

Figure 12. Comparison between the vehicle response in curve to a local or cyclic perturbation: maximum **L/V** ratio on the fourth axle as a function of speed (for level 1, table 1).

For this reason, the next stepwas to consider a cyclic alignment perturbation, with the same amplitudes considered for the local one and with fixed wavelength (**10 m**). Looking at figure 11, it can be observed that, also in this case, the maximum **L/V** increases with speed. However, with respect to the local defect, in this case, the derailment condition is reached not only for level three amplitude (at a lower speed) but also for level two amplitude, at **55 km/h**. A comparison between the vehicle response in a curve to a local or cyclic perturbation is shown in figure 12 (for level one amplitude): it is clearly visible that the rate of growth in the maximum calculated **L/V** ratio is higher for the cyclic perturbation, which therefore appears to be more severe.

In order to understand the reason why the cyclic perturbation is more severe than the local defect with the same amplitude, it is interesting to analyze the results of the numerical simulations for the vehicle running in a tangent track, on cyclic alignment perturbations with different wavelengths (figure 13). In fact, in case of the tangent track, higher speed tests can be simulated. It can be observed that the maximum **L/V** increases with speed and then decreases again. The higher the wavelength, the higher is the vehicle speed, which corresponds to the **L/V** peak. This is obviously related to a resonance phenomenon: the performed simulations showed that the maximum dynamic amplification of the wheel–rail lateral contact force is reached when the excitation frequency associated with the track perturbation wavelength and with the vehicle speed is equal to the bogie yaw eigenfrequency.

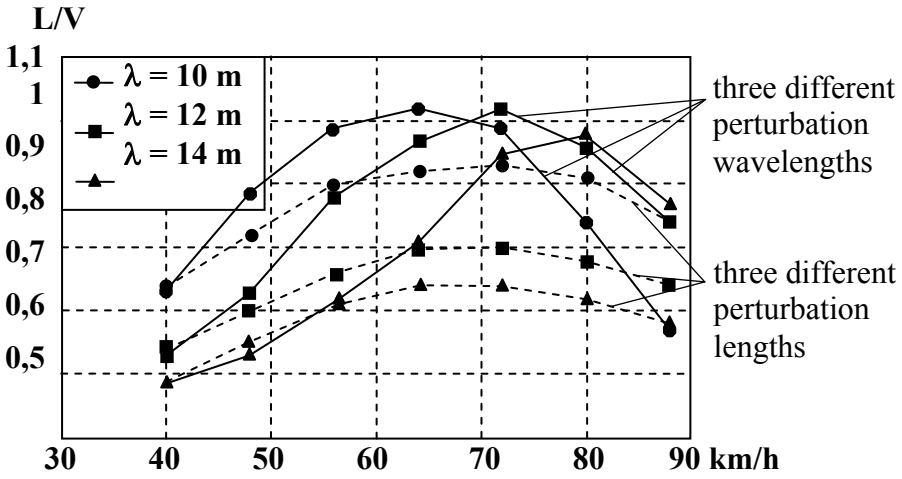

Figure 13. Vehicle response to cyclic alignment perturbation in a tangent track: maximum **L/V** ratio on the fourth axle as a function of speed (three different perturbation wavelengths and three different perturbation lengths).

By performing the same simulations in tangent track, but considering the crossing of a local alignment perturbation (figure 13), the results obtained show a quite different behavior: in this case, for different wavelengths, the shape of the **L/V** curves does not change, thus revealing no dependence on vehicle speed.With the increasing defect's length, the maximum **L/V** values decrease.

7. CONCLUDING REMARKS

For proper analysis of the derailment phenomenon in the real operating conditions, the dynamic effects related to track irregularity excitation must be carefully taken into account.

The parametric analysis presented in this article allows us to point out that, for safe vehicle operation, it is not sufficient to define the limit amplitude of the track geometrical defect as a function of service speed, but also the other defect characteristics (especially the presence of a regular cyclic pattern) must be carefully monitored.

In order to avoid the beginning and/or the growth of the dangerous vehicle–track dynamic interaction phenomena, the operator and the vehicle manufacturer can valuably cooperate: the operator can survey the track maintenance conditions to check for the presence of critical perturbations with respect to the vehicle fleet characteristics, the vehicle manufacturer can verify at design stage if the tramcar suspension can be optimized to reduce sensitiveness to specific line features.

REFERENCES

[1] Belforte, P., Cheli, F., Corradi, R. and Facchinetti, A., Software for the numerical simulation of tramcar vehicle dynamics. Heavy Vehicle Systems, A Special Issue of the International Journal of Vehicle Design, 19, 48–69, 2003

[2] Cheli, F., Corradi, R., Diana, G. and Facchinetti, A., Wheel–rail contact phenomena and derailment conditions in light urban vehicles. Paper presented at the 6th International Conference on Contact Mechanics and Wear of Rail/Wheel Systems (CM2003), Goteborg, Sweden, 2003

[3] Elkins, J.A. and Carter, A., Testing and analysis techniques for safety assessment of rail vehicles: the state-of-the-art. Vehicle System Dynamics, 22, 185–208, 1993

[4] Elkins, J.A. and Wu, H., Angle of attack and distance-based criteria for flange climb derailment. Vehicle System Dynamics (Suppl.), 33, 293–305, 1999

[5] Jovanovic R., Railway vehicles wheelsets, Saobracajni institut CIP, Beograd, 1996

[6] Nenov, N., Ruzhekov T., Mihov G., Dimitrov E., Technology for Dynamic Wheel Load Measuring of Railway Carriages, The 12th International Scientific and Applied Science Conference "Electronics ET'2003", Sozopol 24-26 September, book 1, p64-69

[7] Pascal, J.P. and Sauvage, G., The available methods to calculate the wheel/rail forces in non-hertzian contact patches and rail damaging. Vehicle System Dynamics, 22, 263–275, 1993

[8] Shen, Z.Y., Hedrick, J.K. and Elkins, J.A., A comparison of alternative creep–force models for rail vehicle dynamic analysis. Paper presented at the 8th IAVSD Symposium, Cambridge, MA. 1983

[9] Soskic Zl., Petrovic, Dr., Bogojevic, N., Rakanovic, R., Suggestions for development of sensors for measurement of forces at wheel-rail contact., Mechanics Transport Communications ISSN 1312-3823 issue 1, 2007 article № 0082 http://www.mtc-aj.com